Volume 3 | Number 10 | October 2019

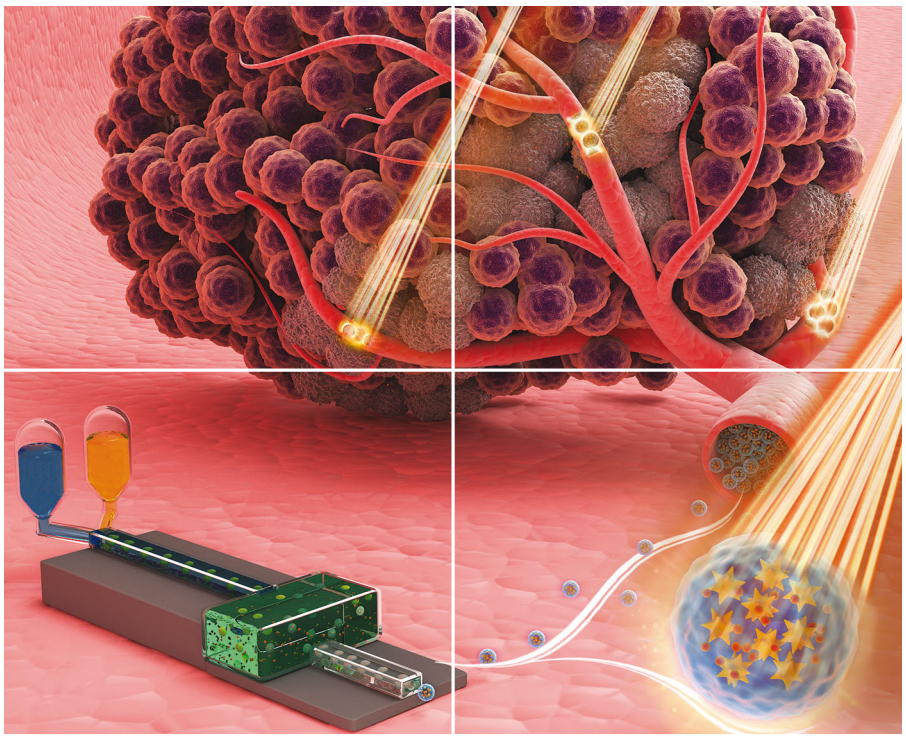

MATERIALS CHEMISTRY

FRONTIERS

CCS 中国化学会 CHINESE CHEMICAL SOCIETY
ICCAS 1956
ROYAL SOCIETY OF CHEMISTRY | Celebrating IYPT 2019
rsc.li/frontiers-materials

MATERIALS CHEMISTRY
FRONTIERS

RESEARCH ARTICLE

View Article Online
View Journal | View Issue

Cite this: *Mater. Chem. Front.*, 2019, **3**, 2018

One-step preparation of multifunctional alginate microspheres loaded with *in situ*-formed gold nanostars as a photothermal agent†

Fangli Hou,‡[a] Yanhong Zhu,‡[b] Qian Zou,[a] Chun Zhang,[b] Hong Wang,[a] Yonggui Liao,[a] Qin Wang,*[a] Xiangliang Yang[b] and Yajiang Yang[a]

Received 29th April 2019,
Accepted 6th June 2019

DOI: 10.1039/c9qm00276f

rsc.li/frontiers-materials

This work is to develop a kind of multifunctional embolic material, which will possess a synergized tumor ablation effect combining transcatheter arterial chemoembolization and hyperthermia therapy. Herein, monodispersed calcium alginate (CA) microspheres containing gold nanostars (Au NSs) have been prepared in one step by using a droplet-based microfluidic technique. The droplets containing sodium alginate (SA) and $HAuCl_4$ formed in the microfluidic device are solidified by Ca^{2+} to obtain CA microspheres while $HAuCl_4$ is successively reduced to Au(0) by SA and vitamin C in the collecting solution to produce Au NSs *in situ*-encapsulated in CA microspheres. Herein, alginate acts as a co-reducing agent and stabilizer for *in situ*-formed Au NSs, and also as a drug carrier and embolic agent. Studies of scanning electronic microscopy combined with energy-dispersive X-ray spectroscopy, transmission electronic microscopy and X-ray diffraction verified the existence and morphology of the *in situ*-formed Au NSs. The as-prepared microspheres can absorb near-infrared (NIR) light and the temperature increment of the microsphere suspension can be more than 60 °C under NIR irradiation due to the presence of Au NSs. The drug release rate can be accelerated by NIR irradiation. The study of *in vitro* cytotoxicity indicates that tumor cells can be efficiently killed by the combination of chemotherapy and NIR-induced hyperthermia. As potential embolic materials, the hybrid microspheres provide new insights into synergistic therapy of cancer.

Introduction

Sodium alginate, as a kind of anionic marine-based biopolymer, possesses well-known advantages such as biocompatibility, biodegradability, low cost, non-toxicity, abundant resources, easy gelation ability and so on.[1,2] Therefore, alginates have been widely used as biomedical materials, particularly in the areas of wound dressing,[3] cell microencapsulation,[4] drug delivery[5] and tissue engineering.[6] Additionally, alginate microsphere suspension as a vascular embolic agent can be injected into tumor sites through a microcatheter to block the nutrition supply to the tumor, resulting in tumor necrosis.[7–10] Meanwhile, anti-cancer drugs loaded within embolic microspheres can be directly delivered to tumor sites with reduced systemic toxicity and high therapeutic efficiency. Therefore, transcatheter arterial chemoembolization (TACE) therapy has been considered as a preferred choice for patients with unresectable liver tumor taking the advantage of embolization combined with local chemotherapy.[11,12]

However, incomplete tumor necrosis and relapse after TACE treatment frequently happened leading to the failure of TACE.[13] In order to improve the therapeutic efficacy of TACE, multimodal treatment combining chemoembolization and other treatments has received great attention recently.[7,14,15] As reported, hyperthermia therapy can kill tumor cells directly and also sensitize radiotherapy and chemotherapy.[16–18] Therein, near-infrared (NIR) light-mediated photothermal therapy (PTT) has been paid much attention due to its unique targeting, minimal invasiveness, high efficacy and low side effect.[19,20] Therefore, TACE combined with photothermal therapy may provide a new strategy to enhance the treatment efficacy because of the tri-modality treatment (PTT, chemotherapy and embolization).

Gold nanostars (Au NSs) have been reported to possess high NIR photothermal conversion efficiency, and also good biocompatibility as well as excellent chemical stability.[21,22]

[a] *Hubei Key Laboratory of Bioinorganic Chemistry & Materia Medica, School of Chemistry and Chemical Engineering, Huazhong University of Science and Technology, Wuhan 430074, People's Republic of China. E-mail: qwang@mail.hust.edu.cn*

[b] *National Engineering Research Center for Nanomedicine, College of Life Science and Technology, Huazhong University of Science and Technology, Wuhan 430074, People's Republic of China*

† Electronic supplementary information (ESI) available: Optical micrographs and the corresponding SEM images of Au@CA microspheres; TEM images of the *in situ*-formed Au NPs in the dispersed phase and in Au@CA microspheres; HRTEM images and the corresponding SAED pattern of the *in situ*-formed Au NS in the microspheres; content of gold in Au@CA microspheres. See DOI: 10.1039/c9qm00276f

‡ These authors contributed equally to this work.

Therefore, combined chemo-photothermal cancer therapy based on Au NSs has been developed in the past decade.[21–25] However, these research studies mainly focused on nanomedicine for systemic intravenous injection therapy. The combination of TACE and NIR photothermal therapy based on Au NSs has never been reported. In addition, the preparation of these multifunctional embolic materials is rather complicated. For instance, Au NSs itself should be synthesized firstly[26–28] and were consequently encapsulated in matrix materials. Therein, the use of a reducing agent and cationic surfactant may cause potential toxicity.[29–31] Therefore, the development of a simple and green method for multifunctional embolic materials based on Au NSs still remains a challenge.

Due to the large number of hydroxyl and carboxyl groups in alginate chains, alginate is capable of reacting with multivalent metal ions or metal nanoparticle *via* electrostatic or coordination interactions. Therefore, alginate is also used as an excellent stabilizer and soft template to synthesize various metal/metal oxide nanocomposites, such as Au, Ag and CeO_2.[32–35] Additionally, as a green and mild reducing agent, alginate is capable of reducing $HAuCl_4$ to Au(0) or $AgNO_3$ to Ag(0) due to the presence of hydroxyl groups.[36–40] But these as-synthesized Au or Ag nanoparticles (NPs) were in spherical shape without NIR photothermal conversion properties.

In this work, monodispersed calcium alginate microspheres containing gold nanostars (denoted as Au@CA) used as embolic materials were prepared in one step by using a droplet-based microfluidic technique. The droplet-based microfluidic technique has emerged as a powerful method to fabricate various microspheres with controllable size and microstructure in the recent two decades.[41] Based on this advanced technique, we have fabricated various monodispersed nano-in-micro hybrid microspheres as potential embolic materials with controllable size and microstructure.[42–45] It is worth noting that gold nanostars (Au NSs) were *in situ*-formed and uniformly distributed in the alginate matrix. Herein, alginate plays a dual role: a co-reducing agent for chloroauric acid and a stabilizer for the consequently formed Au NSs. Furthermore, an anti-cancer drug was loaded within the microspheres. Thus, the as-prepared microspheres may integrate tri-modality treatments including local chemotherapy, thermotherapy and embolization. It is expected to improve the therapeutic effect of TACE. Considering that the embolic effect of hybrid alginate microspheres on VX2 liver tumor-bearing rabbits has been investigated in our previous research,[45] the *in vivo* evaluation of the as-prepared Au@CA microspheres is no longer carried out in this work.

Materials and methods

Materials

Sodium alginate (low viscosity, denoted as SA) was purchased from Sigma-Aldrich. Chloroauric acid ($HAuCl_4 \cdot 3H_2O$) was produced by Reagent No. 1 Factory of Shanghai Chemical Reagent Co. Ltd. DOX hydrochloride (DOX·HCl, 99.3% in purity) was produced by Beijing Huafeng United Technology Co. Ltd. RPMI-1640 medium (BR), penicillin (10^4 U mL^{-1}) and streptomycin (10^4 U mL^{-1}) were purchased from Hyclone. Trypsin (0.25%) and newborn calf serum (NBCS, BR) were obtained from Gibco. Cell Counting Kit-8 (CCK-8, BR) was purchased from Dojindo. Liquid paraffin (CP), span 80 (CP), $CaCl_2$, ascorbic acid (vitamin C) and other chemicals were of analytical grade and purchased from Sinopharm Chemical Reagent Co. Ltd.

Preparation of alginate microspheres containing gold nanostars

According to the method described previously,[43–45] a flow-focused microfluidic device based on polydimethylsiloxane was fabricated. As shown in Fig. 1a, liquid paraffin containing 2 wt% of span 80 and 0.8 wt% *in situ*-formed $CaCl_2$ nanoparticles (NPs) was adopted as a continuous phase, which was prepared using an emulsion process followed by solvent evaporation.[46] The aqueous solution of SA (2.0 wt%) containing varied amounts of $HAuCl_4$ (2.5, 5.0, 10.0 and 20.0 mmol L^{-1}) was stirred in the dark overnight and then used as a dispersed phase. Both the continuous phase and dispersed phase were separately pumped into the microchannels using digitally controlled syringe pumps (NE-1000; New Era Pump Systems, Inc.) with flow rates of 500 μL h^{-1} and 3000 μL h^{-1} respectively. SA droplets containing $HAuCl_4$ were produced and pre-crosslinked with $CaCl_2$ NPs in the microchannel. Meanwhile, a part of $HAuCl_4$ was reduced by alginates to form Au NPs. Subsequently, these droplets were dripped into a collecting solution containing $CaCl_2$ (0.2 mol L^{-1}) and ascorbic acid (vitamin C, 0.05 mol L^{-1}), and were then maintained in the solution for 24 h to ensure complete reaction. Herein, SA droplets were crosslinked with Ca^{2+} ions to form calcium alginate (CA) hydrogel microspheres and $HAuCl_4$ was further reduced to Au NSs by vitamin C. The resultant CA microspheres containing *in situ*-formed Au NSs (denoted as Au@CA) were collected and purified by washing several times with alcohol and DI water alternately. According to the content of $HAuCl_4$ added in the dispersed phase, the resultant CA microspheres were denoted as Au@CA-2.5, Au@CA-5, Au@CA-10 and Au@CA-20. As a control, blank CA microspheres were also prepared using a similar method. These microspheres were either dried in an oven for further characterization, or dispersed in water for storage.

Morphology and structure of Au@CA microspheres

The morphologies of the various wet microspheres were observed using an inverted optical microscope (DSY5000X, Chongqing COIC Industrial Co. Ltd). The freeze-dried microspheres were gold-coated before imaging on an environmental scanning electron

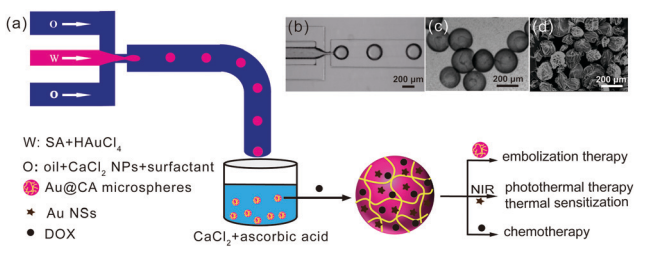

Fig. 1 (a) Schematic illustration of one-step preparation of Au@CA microspheres with a nano-in-micro structure; (b) optical micrograph of the droplets formation in the microfluidic device; (c and d) optical photograph and SEM image of Au@CA microspheres.

microscope (ESEM, Quanta 200, FEI) at an accelerating voltage of 10 kV. The elemental composition of the microspheres were analysed using SEM combined with energy dispersive X-ray spectroscopy (SEM-EDX, Genesis, EDAX Inc.). The operation voltage was 20 kV. The micromorphology of the *in situ*-formed Au NPs in microspheres was imaged by using a field transmission electron microscope (Tecnai G2 F30, FEI) with an accelerating voltage of 160 kV. Briefly, the dried microspheres were ground into powder and disintegrated using EDTA solution (0.1 mol L^{-1}) under ultrasonication. Au NSs were leached out from the microspheres and collected by centrifugation (12 000 rpm, 15 min). The obtained Au NSs were then spread onto an ultra-thin carbon film coated copper grid and dried for tests. High-resolution TEM (HRTEM) images and selected area electron diffraction (SAED) patterns of Au NSs were obtained with an accelerating voltage of 300 kV.

The crystal structures of the Au@CA microspheres were also measured using a powder X-ray diffraction instrument (XRD, X'Pert PRO, PANalytical B.V.) with 2θ ranging from 10.0° to 80.0° under Cu Kα radiation. The thermal stability of the microspheres was investigated on a thermal gravimetric analyzer (TGA, Pyris1, PerkinElmer) under a N_2 atmosphere with a temperature range of 28–850 °C and heating rate of 10 °C min^{-1}. The contents of Au in the microspheres were determined using an atomic absorption spectrometer (AAS, iCE 3000, Thermo Scientific). Precisely weighed and dried microspheres were firstly dissolved in a mixture of aqua regia (8 mL) and H_2O_2 (0.5 mL). Then the obtained system was placed on an electric heat plate at 150 °C for 2 h to get rid of the acid and then volumized, filtered through a ∅ 0.45 μm membrane and diluted before the test. The absorption intensity at 242.8 nm was recorded and the content of Au was calculated according to the standard curve of Au.

Spectral analysis of Au@CA microspheres

The absorption spectra of Au@CA microspheres and the dispersed phase containing $HAuCl_4$ were examined on a UV-vis-NIR spectrometer (UV-3600, Shimadzu). Before the test, the microspheres were firstly disintegrated in EDTA (0.1 mol L^{-1}). The obtained suspensions were scanned from 300–1100 nm using 0.1 mol L^{-1} EDTA as a reference. Both scan models were in high speed with an interval of 1 nm.

In vitro photothermal effects of Au@CA microspheres

A digital thermometer (DM6801A, Shenzhen Victory Electronic Technology Co. Ltd) and an infrared camera (FLIR E50, FLIR Systems Inc.) were employed to monitor the temperature change. Briefly, various dried microspheres (20 mg) were placed in a 96-well plate and swollen with 200 μL of DI water separately. Subsequently, the suspensions of microspheres were irradiated using a 808 nm laser (MW-GX-808/5000 mW, Changchun Laser Optoelectronics Technology Co. Ltd) with varied power densities. The spot diameter of the laser was 1 cm. The vertical distance between the sample and laser was approximately 10 cm.

Drug loading and *in vitro* release of Au@CA microspheres

DOX·HCl was used as a model drug in this study. DOX-loaded microspheres were prepared using a swelling adsorption method.[47] Briefly, ~95 mg of freeze-dried microspheres were immersed in 4 mL of DOX·HCl (4 mg mL^{-1}) solution. The microsphere suspension was oscillated at a rate of 100 rpm at 37 °C for 48 h. Subsequently, the suspension was centrifuged and washed with DI water till a colourless supernatant was obtained. The drug-loaded microspheres were dried in an oven for further use. All supernatants of centrifugation were collected together and diluted to a constant volume. The drug loading capacity (LC) and encapsulation efficiency (EE) of the microspheres were calculated according to the measured concentration of free DOX and initial DOX concentration. The obtained DOX-loaded Au@CA-10 and CA microspheres were denoted as DOX-Au@CA-10 and DOX-CA microspheres, respectively. All the procedures involving DOX were performed in the dark.

In vitro release profiles of DOX from the microspheres were obtained by a dialysis method.[47] Briefly, the weighed and freeze-dried drug-loaded microspheres (~10 mg) were placed in a dialysis bag (the cut-off molecular weight was 14 000 Da) with 1 mL of phosphate-buffered solution (PBS, pH 7.4, 0.01 mol L^{-1}). The dialysis bag was immersed in 19.0 mL of PBS in a capped flask and placed on an oscillator with a rate of 100 rpm at 37 °C. At a designed time interval, 4.0 mL of the release medium was removed and replaced with an equal volume of fresh medium. The amount of the released DOX was quantified by measuring the absorbance of the release medium on a UV-visible spectrophotometer (UV-2550, Shimadzu) at a wavelength of 480 nm based on a DOX standard curve.

To investigate the effect of NIR laser irradiation on the drug release behaviour of the microspheres, the dialysis bag containing the microsphere suspension was removed from the flask at a designated time interval and irradiated with a NIR laser (808 nm, 1.0 W cm^{-2}). The time of irradiation was 5 min at time points of 3, 4 and 5 h, and 10 min at time points of 22, 23 and 24 h, respectively. The diameter of the laser collimator was 2 cm. The distance between the dialysis bag and laser head was set as 5 cm. All the drug release tests were performed in triplicate.

In vitro cytotoxicity of Au@CA microspheres

The cytotoxicity of the microspheres was evaluated by CCK-8 assay using human hepatocellular (HepG2) cells.[43] Briefly, the cells were seeded in a 96-well plate at a density of 8×10^3 cells per well and then incubated overnight. The dried microspheres were swollen and dispersed in the culture medium. The content of microspheres was ~0.5 mg mL^{-1}. Subsequently, 200 μL of the microsphere dispersion was added into wells. For groups of NIR irradiation, laser irradiation (808 nm, 1.5 W cm^{-2}) was carried out immediately for 3 min per well. After 24 h of incubation, 10 μL of CCK-8 was added to each well and the cells were further incubated for 4 h. The absorbance was measured using a Microplate Reader (Model 680, BIO-RAD, USA) at a wavelength of 450 nm.

Statistical analysis

The data were presented as mean ± standard deviation (SD). Statistical analyses were performed by Student's *t*-test. Symbols ** and *** indicated $P < 0.01$ and $P < 0.001$ with considered significant differences, respectively.

Results and discussion

Preparation and characterization of Au@CA microspheres

Fig. 1 schematically shows the one-step preparation of hybrid CA microspheres containing *in situ*-formed Au NPs *via* a droplet-based microfluidic technique. The subsequent morphology and structure characterization showed that Au NPs encapsulated in the CA microspheres were in the shape of multi-antenna nanostars (NSs). Hereafter, in this paper, if the shape of the Au nanoparticles is indeterminate, they would be called Au NPs. And Au NSs would be used to refer in particular to Au NPs with the shape of nanostars. Au NSs can absorb NIR light and act as a NIR photothermal agent. In addition, DOX was used as the chemotherapy drug loaded in the microspheres using an adsorption method. Thus, the obtained drug-loaded hybrid microspheres may integrate embolization therapy, hyperthermia therapy and local chemotherapy. As shown in Fig. 1a, a flow-focusing microfluidic device allows obtaining monodispersed sodium alginate (SA) droplets firstly (Fig. 1b). In the microchannel, SA droplets were pre-crosslinked with $CaCl_2$ NPs in a continuous phase (O) as we reported previously.[46] In addition, a part of $HAuCl_4$ in the dispersed phase (W) could be *in situ* reduced to Au NPs due to the reduction ability of SA. The droplets were dripped into a collecting bath containing $CaCl_2$ and vitamin C. Herein, SA was completely solidified by Ca^{2+} to form calcium alginate (CA); simultaneously, unreacted $HAuCl_4$ was further *in situ* reduced to Au NSs by vitamin C. Thus, such hybrid CA microspheres with a unique nano-in-micro structure were prepared by a simple one-step method. The resultant hybrid CA microspheres were denoted as Au@CA microspheres. Among the as-prepared samples, the size of Au@CA-10 microspheres was found to be approximately 200 μm with monodispersion (Fig. 1c), which is suitable to be an embolic agent and can be easily modulated by adjusting the flow rates of both phases to meet the different requirements. The SEM image indicated that the size of the dried microspheres was approximately 150 μm (Fig. 1d). The shape and size of the other hybrid microspheres are shown in Fig. S1 in ESI.†

The existence of Au in the hybrid microspheres was verified by SEM combined with EDX as shown in Fig. 2. In comparison with the clear surface of the blank CA microsphere (Fig. 2a), a number of white particles with uniform size can be clearly observed on the surface of Au@CA-10 microspheres (Fig. 2b). These white particles could be considered to be *in situ*-formed Au NPs. Their morphology would be characterized *vide infra*. These Au NPs well dispersed in the matrix of CA due to the soft

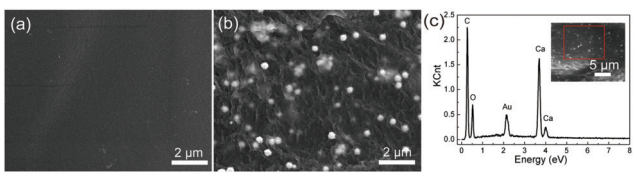

Fig. 2 (a) SEM image of the surface of blank CA microspheres; (b) SEM image of the surface of Au@CA-10 microspheres; and (c) EDX analysis of Au@CA-10 microspheres based on a selected area (red square) of the SEM image.

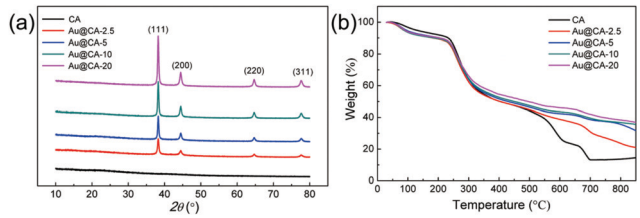

Fig. 3 (a) XRD patterns and (b) thermogravimetric analysis of various CA microspheres.

template effect of alginate network structures. The aggregation and precipitation of Au NPs were also avoided by such a template effect.[32–35] As shown in Fig. 2c, EDX analysis of Au@CA-10 microspheres verified the existence of elements C, O, Ca and Au in the matrix of alginate. The content of element Au in Au@CA-10 microspheres was found to be 10.4 wt%.

Fig. 3 shows the XRD spectra and thermogravimetric analysis of various CA microspheres. In Fig. 3a, according to the standard XRD data JCPDS card 04-078 (face-centered cubic phase), the peaks at 38.3°, 44.5°, 64.7° and 77.7° were assigned to the (111), (200), (220) and (311) crystal planes of Au, respectively.[48] However, no peak in the range of 10.0–80.0° was observed in the case of blank CA microspheres. In addition, the ratio of the peak intensity of (111) and (200) was about 3.49, which was higher than 2.20 as indicated in the JCPDS standard card. This may suggest that the crystal of Au mainly grows along the (111) crystal plane. Fig. 3b shows the thermal decomposition behaviors of various CA microspheres. The thermogravimetric curves of all microspheres were similar in the range of 0–330 °C. With a further increase in temperature, thermal decomposition rates of the samples containing Au gradually slowed down depending upon the content of Au. The results of thermogravimetric analysis also verified the presence of Au in CA microspheres.

In order to illustrate the morphology, properties and the formation mechanism of Au NPs in the hybrid CA microspheres, TEM and absorption spectroscopy of Au NPs in the dispersed phase and in the microspheres were conducted respectively. As shown in Fig. 4a, near spherical Au NPs were obtained from the dispersed phase containing 10 mmol L^{-1} $HAuCl_4$, which might come from a part of $HAuCl_4$ reduced by SA (TEM images of Au NPs obtained from the other dispersed phases can be found in Fig. S2a in ESI†).

The sizes of these Au NPs were 60–80 nm. The corresponding UV-vis-NIR absorption spectra are shown in Fig. 4b. As expected, no absorption peak appeared in the case of the dispersed phase without $HAuCl_4$. However, strong absorption peaks appeared at ~550 nm when the dispersed phases contained varied contents of $HAuCl_4$. This might be attributed to the formation of Au NPs during the preparation of the dispersed phase due to the mild reducing capability and soft template effect of alginate as mentioned above. Fig. 4c shows the TEM image of Au NPs obtained from the disintegrated Au@CA-10 microspheres (TEM images of other samples are shown in Fig. S2b, ESI†). In comparison with the spherical Au NPs obtained from the dispersed phase, Au NPs in the CA microspheres showed a

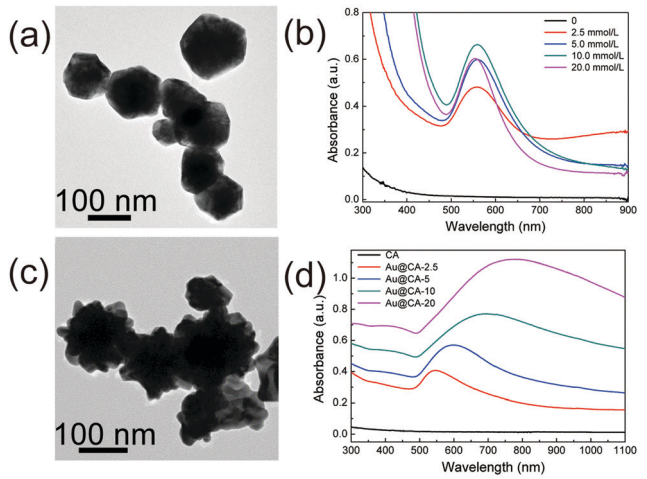

Fig. 4 (a and c) TEM image of Au NPs; (b and d) the corresponding UV-vis-NIR absorption spectra of the Au NPs suspension. (a and b) From the dispersed phases; (c and d) from the disintegrated microspheres.

multi-tentacle star-like shape. Thus, these Au nanoparticles were denoted as Au nanostars (Au NSs). The size of Au NSs seemed to be larger than that of the above spherical Au NPs in the corresponding dispersed phase and had a tendency to increase with an increase in $HAuCl_4$ content in the dispersed phase. For instance, the size of the Au NSs in Au@CA-2.5 was about 70 nm, while that in Au@CA-20 was about 150 nm (Fig. S2b, ESI†). Fig. 4d shows the corresponding UV-vis-NIR spectra of Au NS suspensions obtained from the disintegrated Au@CA-2.5, Au@CA-5, Au@CA-10 and Au@CA-20 microspheres. Their absorption peaks appeared at 550 nm, 610 nm, 700 nm and 780 nm, respectively. In comparison with that of near spherical Au NPs obtained from the dispersed phases, the absorption peaks of the Au NS suspension shifted to the near-infrared region, which might be due to their multi-tentacle star-like shape. Interestingly, such a redshift was also related to the content of $HAuCl_4$, alternately, related to the size of Au NSs. Namely, the higher the $HAuCl_4$ content in the dispersed phase, the bigger the size of the Au NSs and the larger the redshift of the absorption peak. In addition, the crystal phase and structure of the *in situ*-formed Au NSs in the CA microspheres were further characterized using HRTEM combined with SAED (Fig. S3, ESI†). A clear lattice fringe with a spacing of 0.23 nm was found (Fig. S3a and c, ESI†), which corresponded to the (111) crystal plane. Fig. S3b and d (ESI†) indicated that the *in situ*-formed Au NSs possessed a polycrystalline feature.

From the above results and discussion, we proposed that the formation of Au NSs might experience a process of nucleation in the dispersed phase and crystal growth in the collecting solution. In the dispersed phase, a small amount of $HAuCl_4$ was reduced by SA to form near spherical Au NPs. Then, the residual $HAuCl_4$ was further reduced to Au by vitamin C in the collecting solution and these formed Au deposited preferentially on the (111) crystal plane of the initially generated spherical Au NPs, ultimately leading to the formation of multi-antenna Au nanostars in the CA microspheres. In this process, alginate chains act as a soft template to prevent the aggregation and precipitation of Au NPs. Unlike the reported two-step preparation of Au NSs,[29–31] extra surfactant and careful control of reaction conditions were not required. Au content in Au@CA microspheres was also evaluated by using the AAS method (Table S1, ESI†). As expected, the Au content in these microspheres increased with an increase of $HAuCl_4$ concentration in the dispersed phase.

In vitro photothermal effect of Au@CA microspheres

As demonstrated above, Au NSs were encapsulated in CA microspheres and showed strong absorption in the NIR region. This implies that Au@CA microspheres are capable of photothermal conversion.[21,22] Fig. 5 shows the temperature increments (ΔT) of various microsphere suspensions irradiated using a 808 nm NIR laser. In comparison with very small ΔT in the case of water and pure CA microsphere suspension, distinct temperature increments were observed in the case of Au@CA microsphere suspensions (Fig. 5a). The ΔT in the case of CA, Au@CA-2.5, Au@CA-5, Au@CA-10 and Au@CA-20 microsphere suspensions was found to be 11, 23, 27, 33 and 41 °C, respectively, under irradiation with a power of 0.50 W cm^{-2} for 15 min. It is indicative that the ΔT increased with an increase of Au content. It is worth noting that the power density (0.50 W cm^{-2}) is relatively low, but is able to produce significant ΔT. In this work, we also investigated the effect of power density on ΔT for various microsphere suspensions. As shown in Fig. 5b, ΔT of the Au@CA-10 suspension increased with an increase in the power density of the laser. Under NIR irradiation with power densities of 0.25, 0.50, 0.80 and 1.00 W cm^{-2}, the corresponding ΔT of Au@CA-10 microspheres was found to be 29, 48, 61 and 67 °C, respectively, much higher than those of DI water

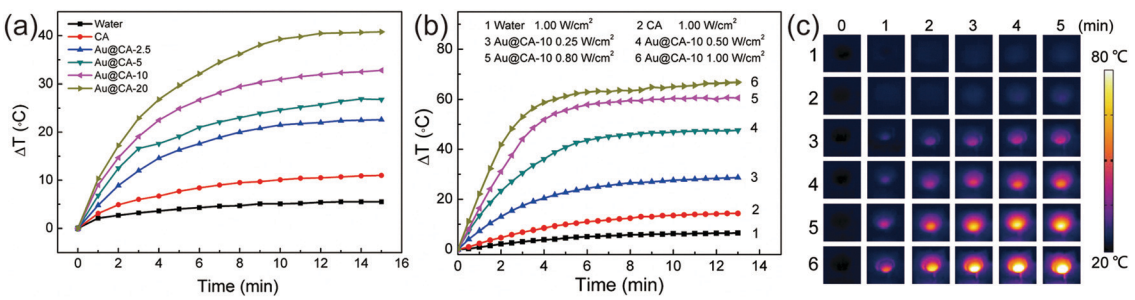

Fig. 5 Photothermal effects. (a) Effect of Au content; (b) effect of the laser power density; and (c) corresponding thermal images of microspheres recorded using an IR camera within 5 min of NIR irradiation.

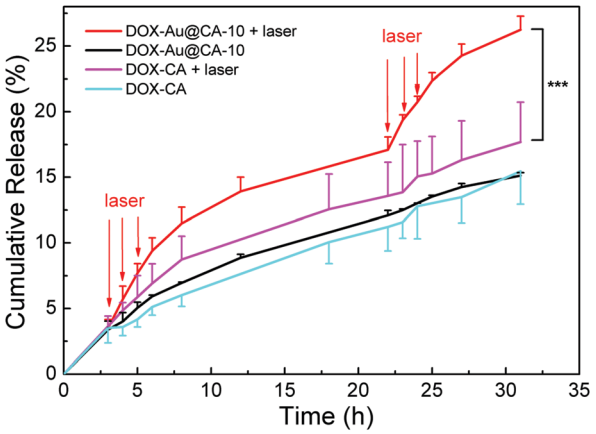

Fig. 6 *In vitro* release behavior of DOX-loading microspheres with or without laser irradiation. Note: ***$P < 0.001$ with significant difference.

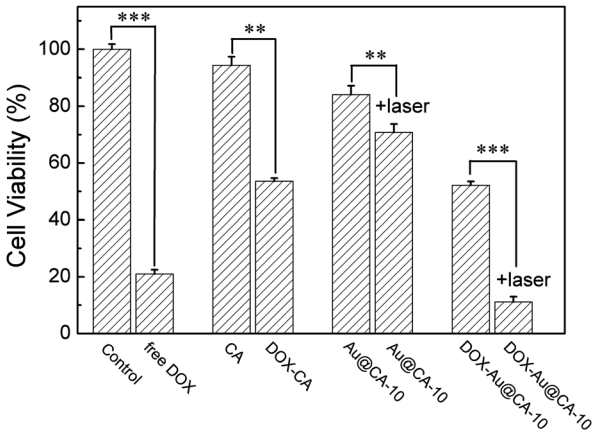

Fig. 7 Cell viabilities of HepG2 cells incubated with various CA microspheres after 24 h. Note: **$P < 0.01$, ***$P < 0.001$ with significant difference, respectively.

and pure CA microspheres. The corresponding thermal images are shown in Fig. 5c. The bright image implies high temperature and *vice versa*. The images were consistent with the monitored temperatures.

Drug loading and *in vitro* release of Au@CA microspheres

The drug loading capacities (LC) of DOX-Au@CA-10 and DOX-CA microspheres were found to be 15.9 ± 0.23% and 16.6 ± 0.03%, respectively. Correspondingly, their encapsulation efficiencies (EE) were found to be 95.2 ± 1.19% and 98.5 ± 0.14%, respectively. The high values of EE might involve hydrogen bonding between DOX and CA, and electrostatic attraction between amino groups in DOX and carboxyl groups in CA. As shown in Fig. 6, both microspheres exhibited almost parallel sustained drug release behavior in the absence of NIR irradiation. It is indicative that the existence of Au NSs doesn't affect the release of the drug. When the NIR laser was employed, a significantly enhanced release rate was observed in the case of DOX-Au@CA-10 microspheres. For instance, about 10% of DOX could be released from the microspheres after 5 h. However, in the absence of irradiation, this release ratio was realized after 17 h. Apparently, the accelerated diffusion of drug molecules from the microspheres could be attributed to the high temperature caused by the photothermal effect of Au NSs in CA microspheres. At the beginning of the release (0–4 h), DOX release could be attributed to the spontaneous molecular diffusion in the absence of irradiation. However, the release rate of DOX distinctly increased when NIR irradiation was applied (3–5 h). When the laser was shut off (6–22 h), the drug release was still driven by spontaneous diffusion. When the irradiation was applied again (22–24 h), the release rate was accelerated again. This indicates that a pulse release of DOX could be conveniently realized through a simple "on–off" of laser irradiation.

In vitro cell viability assay of Au@CA microspheres

Fig. 7 shows the results of *in vitro* cytotoxicity of the as-prepared CA microspheres. After being treated with CA and Au@CA-10 microsphere suspension, the cell viability was 94% and 84%, respectively, implying that these microspheres possess good biocompatibility. When the cells were treated using DOX-Au@CA-10 microspheres, the cell viability was 52%, which was attributed to the release of DOX. However, the cell viability was further decreased to 11% in the case of Au@CA-10 combined with NIR irradiation. It was indicative that more tumor cells were killed by the heat arising from the photothermal conversion of Au NSs in the microspheres. The group of DOX-Au@CA-10 microspheres with NIR irradiation showed a synergistic antitumor effect of chemotherapy and thermotherapy.

Conclusion

A series of calcium alginate microspheres containing *in situ*-formed Au nanostars have been prepared in one step using a droplet-based microfluidic technique. The prepared microspheres have a spherical shape and uniform size with a diameter of about 200 μm in the wet state. Au NSs were formed from the reduction of $HAuCl_4$ by alginate in the dispersed phase (nucleation) and subsequently by vitamin C in the collecting solution (crystal selective growth). The content of *in situ*-formed Au NSs can be adjusted by changing the initial concentration of $HAuCl_4$ in the dispersed phase. The as-prepared nano-in-micro microspheres show an excellent photothermal effect because Au NSs are able to transfer light energy to thermal energy under NIR laser irradiation. In addition, the drug release rate from the microspheres can be accelerated by NIR laser irradiation. The drug-loaded Au@CA microspheres combined with NIR irradiation show a synergistic antitumor effect of chemotherapy and thermotherapy. These results show that Au@CA microspheres have the potential to be used as a multifunctional embolic agent.

Conflicts of interest

There are no conflicts to declare.

Acknowledgements

This work was financially supported by the National Natural Science Foundation of China (grant 51473057 and 81573013).

We thank the Analytical and Testing Centre in Huazhong University of Science and Technology (HUST) and Testing Center in School of Chemistry and Chemical Engineering, HUST for the related measurements.

References

1 K. Y. Lee and D. J. Mooney, *Prog. Polym. Sci.*, 2012, **37**, 106–126.
2 K. I. Draget and C. Taylor, *Food Hydrocolloids*, 2011, **25**, 251–256.
3 B. A. Aderibigbe and B. Buyana, *Pharmaceutics*, 2018, **10**, 42.
4 S. Giovagnoli, G. Luca, P. Blasi, F. Mancuso, A. Schoubben, I. Arato, M. Calvitti, G. Falabella, G. Basta, M. Bodo, R. Calafiore and M. Ricci, *Curr. Pharm. Des.*, 2015, **21**, 4917–4935.
5 M. Lopes, B. Abrahim, F. Veiga, R. Seica, L. M. Cabral, P. Arnaud, J. C. Andrade and A. J. Ribeiro, *Expert Opin. Drug Delivery*, 2017, **14**, 769–782.
6 J. Venkatesan, I. Bhatnagar, P. Manivasagan, K. H. Kang and S. K. Kim, *Int. J. Biol. Macromol.*, 2015, **72**, 269–281.
7 C. H. Fu, F. He, L. F. Tan, X. L. Ren, W. Zhang, T. L. Liu, J. Z. Wang, J. Ren, X. D. Chen and X. W. Meng, *Nanoscale*, 2017, **9**, 14846–14853.
8 C. Oerlemans, P. R. Seevinck, M. L. Smits, W. E. Hennink, C. J. G. Bakker, M. A. A. J. van den Bosch and J. F. W. Nijsen, *Int. J. Pharm.*, 2015, **482**, 47–53.
9 T. A. Becker, D. R. Kipke, M. C. Preul, W. D. Bichard and C. G. McDougall, *Neurosurgery*, 2002, **51**, 453–458.
10 J. J. Rong, M. Liang, F. Q. Xuan, J. Y. Sun, L. J. Zhao, H. Z. Zheng, X. X. Tian, D. Liu, Q. Y. Zhang, C. F. Peng, F. Li, X. Z. Wang, Y. L. Han and W. T. Yu, *Int. J. Biol. Macromol.*, 2017, **104**, 1302–1312.
11 E. Lanza, M. Donadon, D. Poretti, V. Pedicini, M. Tramarin, M. Roncalli, H. Rhee, Y. N. Park and G. Torzilli, *Liver Cancer*, 2017, **6**, 27–33.
12 C. D. Gadaleta and G. Ranieri, *Crit. Rev. Oncol. Hemat.*, 2011, **80**, 40–53.
13 J. Y. J. Huang, S. Kafy, A. Dugas, D. Valenti and T. Tulandi, *Fertil. Steril.*, 2006, **85**, 30–35.
14 H. Yu, G.-Y. Zhu, R.-Z. Xu, H.-Z. Niu, Q. Lu, G.-Z. Li, Z.-Y. Wang, D.-S. Zhang, N. Gu and G.-J. Teng, *PLoS One*, 2011, **6**(3), e17926.
15 S. W. Kwan, W. P. Harris, L. S. Gold and P. L. Hebert, *AJR, Am. J. Roentgenol.*, 2018, **210**, 1359–1365.
16 L. Wang, X. Lin, J. Wang, Z. Hu, Y. Ji, S. Hou, Y. Zhao, X. Wu and C. Chen, *Adv. Funct. Mater.*, 2014, **24**, 4229–4239.
17 M. B. Zheng, C. X. Yue, Y. F. Ma, P. Gong, P. F. Zhao, C. F. Zheng, Z. H. Sheng, P. F. Zhang, Z. H. Wang and L. T. Cai, *ACS Nano*, 2013, **7**, 2056–2067.
18 Q. Liu, Y. Qian, P. Li, S. Zhang, J. Liu, X. Sun, M. Fulham, D. Feng, G. Huang, W. Lu and S. Song, *Theranostics*, 2018, **8**, 785–799.
19 Z. J. Zhang, J. Wang and C. H. Chen, *Adv. Mater.*, 2013, **25**, 3869–3880.
20 H. Kim, S. Beack, S. Han, M. Shin, T. Lee, Y. Park, K. S. Kim, A. K. Yetisen, S. H. Yun, W. Kwon and S. K. Hahn, *Adv. Mater.*, 2018, **30**, 1701460.
21 Y. Liu, H. Yuan, A. M. Fales, J. K. Register and T. Vo-Dinh, *Front. Chem.*, 2015, **3**, 51.
22 X. Yang, M. Yang, B. Pang, M. Vara and Y. Xia, *Chem. Rev.*, 2015, **115**, 10410–10488.
23 G. Su, D. Miao, Y. Yu, M. Zhou, P. Jiao, X. Cao, B. Yan and H. Zhu, *J. Drug Targeting*, 2018, 1–10.
24 Y. Liu, X. Zhi, M. Yang, J. Zhang, L. Lin, X. Zhao, W. Hou, C. Zhang, Q. Zhang, F. Pan, G. Alfranca, Y. Yang, J. M. de la Fuente, J. Ni and D. Cui, *Theranostics*, 2017, **7**, 1650–1662.
25 P. Wei, J. Chen, Y. Hu, X. Li, H. Wang, M. Shen and X. Shi, *Adv. Healthcare Mater.*, 2016, **5**, 3203–3213.
26 W. Niu, Y. A. Chua, W. Zhang, H. Huang and X. Lu, *J. Am. Chem. Soc.*, 2015, **137**, 10460–10463.
27 N. Ahmad, G. Wang, J. Nelayah, C. Ricolleau and D. Alloyeau, *Nano Lett.*, 2017, **17**, 4194–4201.
28 N. N. Zhao, L. S. Li, T. Huang and L. M. Qi, *Nanoscale*, 2010, **2**, 2418–2423.
29 S. V. Sheen Mers, S. Umadevi and V. Ganesh, *ChemPhysChem*, 2017, **18**, 1358–1369.
30 H. L. Wu, C. H. Chen and M. H. Huang, *Chem. Mater.*, 2009, **21**, 110–114.
31 X. Meng, A. Baride and C. Jiang, *Langmuir*, 2016, **32**, 6674–6681.
32 Z. Schnepp, S. R. Hall, M. J. Hollamby and S. Mann, *Green Chem.*, 2011, **13**, 272–275.
33 P. Sierra-Rosales, R. Torres, C. Sepulveda, M. J. Kogan and J. A. Squella, *Electroanalysis*, 2018, **30**, 386–396.
34 S. Dey, M. C. D. Sherly, M. R. Rekha and K. Sreenivasan, *Carbohydr. Polym.*, 2016, **136**, 71–80.
35 S. Y. Seo, G. H. Lee, S. G. Lee, S. Y. Jung, J. O. Lim and J. H. Choi, *Carbohydr. Polym.*, 2012, **90**, 109–115.
36 L. Zhao, J. J. Song, Y. Xue, X. H. Zhao, Y. J. Deng, Q. Li and Y. Z. Xia, *Catal. Lett.*, 2018, **148**, 3248–3256.
37 X. H. Zhao, Z. C. Li, Y. J. Deng, Z. H. Zhao, X. W. Li and Y. Z. Xia, *Materials*, 2017, **10**, 557.
38 D. Sahu, N. Sarkar, G. Sahoo, P. Mohapatra and S. K. Swain, *Sens. Actuators, B*, 2017, **246**, 96–107.
39 Q. J. Li, A. A. Sun, Y. S. Si, M. Chen and L. M. Wu, *Chem. Mater.*, 2017, **29**, 6758–6765.
40 X. H. Zhao, Y. Z. Xia, Q. Li, X. M. Ma, F. Y. Quan, C. Z. Geng and Z. Y. Han, *Colloids Surf., A*, 2014, **444**, 180–188.
41 L. R. Shang, Y. Cheng and Y. J. Zhao, *Chem. Rev.*, 2017, **117**, 7964–8040.
42 Q. Wang, D. Zhang, X. L. Yang, H. B. Xu, A. Q. Shen and Y. J. Yang, *Green Chem.*, 2013, **15**, 2222–2229.
43 Q. Wang, A. Xiao, Y. Liu, Q. Zou, Q. Zhou, H. Wang, X. Yang, C. Zheng, Y. Yang and Y. Zhu, *Nanomedicine*, 2018, **14**, 2551–2561.
44 Q. Wang, D. Zhang, H. Xu, X. Yang, A. Q. Shen and Y. Yang, *Lab Chip*, 2012, **12**, 4781–4786.
45 Q. Wang, K. Qian, S. S. Liu, Y. J. Yang, B. Liang, C. S. Zheng, X. L. Yang, H. B. Xu and A. Q. Shen, *Biomacromolecules*, 2015, **16**, 1240–1246.
46 Q. Wang, S. Liu, H. Wang, J. Zhu and Y. Yang, *Colloids Surf., A*, 2015, **482**, 371–377.
47 Q. Wang, S. Liu, F. Yang, L. Gan, X. Yang and Y. Yang, *Int. J. Nanomed.*, 2017, **12**, 4335–4347.
48 Y. Y. Ma, J. S. Wan, K. Qian, S. N. Geng, N. J. He, G. F. Zhou, Y. B. Zhao and X. L. Yang, *J. Mater. Chem. B*, 2014, **2**, 6044–6053.

